Gao et al. Nanoscale Research Letters (2015) 10:176
DOI 10.1186/s11671-015-0874-7

Nanoscale Research Letters
a SpringerOpen Journal

NANO EXPRESS Open Access

Novel hollow α-Fe_2O_3 nanofibers via electrospinning for dye adsorption

Qiang Gao[1,2*], Jun Luo[1], Xingyue Wang[1], Chunxia Gao[1,3*] and Mingqiao Ge[1]

Abstract

Nanomaterials such as iron oxides and ferrites have been intensively investigated for water treatment and environmental remediation applications. In this work, hollow α-Fe_2O_3 nanofibers made of rice-like nanorods were successfully synthesized via a simple hydrothermal reaction on polyvinyl alcohol (PVA) nanofiber template followed by calcination. The crystallographic structure and the morphology of the as-prepared α-Fe_2O_3 nanofibers were characterized by X-ray diffraction, energy dispersive X-ray spectrometer, and scanning electron microscope. Batch adsorption experiments were conducted, and ultraviolet-visible spectra were recorded before and after the adsorption to investigate the dye adsorption performance. The results showed that hollow α-Fe_2O_3 fiber assembles exhibited good magnetic responsive performance, as well as efficient adsorption for methyl orange in water. This work provided a versatile strategy for further design and development of functional nanofiber-nanoparticle composites towards various applications.

Keywords: Hollow nanofiber; Electrospinning; α-Fe_2O_3; Magnetic

Background

In recent decades, magnetic iron oxide has developed into a kind of nanomaterial with the property of magnetic targeting [1,2]. α-Fe_2O_3 has attracted considerable attention due to its widely applications, such as catalysis [3-5], batteries [6,7], and gas sensors [8,9]. Recently, much effort has been devoted to the design and controllable synthesis of one-dimensional (1D) nanostructure α-Fe_2O_3 due to the novel properties of nanoscale materials. Liu et al. synthesized α-Fe_2O_3 nanotubes by a templating method [10]. Jiang's group and Gou's research group have fabricated α-Fe_2O_3 nanofibers via electrospinning, respectively [11,12].

Electrospinning is a simple method for producing nanofibers and nonwovens for various applications [13-16]. Electrospinning is advantageous to fabricate not only solid nanofibers but also hollow nanofibers. The main strategies adopted for hollow nanofiber synthesis via electrospinning are as follows: (1) *Coaxial electrospinning* involves the use of two coaxial capillaries in a spinneret containing different solutions to generate core-shell composite fibers that results in hollow fibers via removal of core fibers by extraction or calcination at high temperature [17,18]. (2) *Single nozzle co-electrospinning*: this process involves two immiscible polymers dissolved in solvent that results in phase separation during electrospinning owing to the intrinsic polymer properties, yielding core-shell composite fibers or hollow fibers after suitable core removal [19,20]. However, inorganic hollow fiber with hierarchical structure is hard to be achieved via the two mentioned methods.

Nanoscale α-Fe_2O_3 has been intensively investigated for water treatment and environmental remediation applications [21-23]. Song et al. reported that flowerlike α-Fe_2O_3 nanoparticles can remove the heavy metal ions from the waste water [21]. Grätzel et al. employed nanostructured α-Fe_2O_3 films for azo-dye adsorption [22]. Yu et al. investigated the methyl orange degradation performance by using α-Fe_2O_3 nanocrystals [23]. To the best of our knowledge, there are no reports in the literature dealing with interconnected α-Fe_2O_3 hollow fibers for dye adsorption in the waste water. In this work, we have synthesized a interconnected 1D hollow structure of α-Fe_2O_3 nanofibers made of rice-like nanorods by annealing electrospun polyvinyl alcohol (PVA)-Fe_3O_4

* Correspondence: gaoqiang@jiangnan.edu.cn; cxgao@suda.edu.cn
[1]Key Laboratory of Science and Technology of Eco-Textiles, Ministry of Education, Jiangnan University, 1800 Lihu Road, Wuxi 214122, China
[3]Institute of Orthopaedics, The First Affiliated Hospital, Soochow University, 708 Renmin Road, Suzhou 215006, China
Full list of author information is available at the end of the article

composite fibers and investigated its potential applications in removal of noxious dye from wastewater.

Methods

Materials

99.9% hydrolyzed PVA samples (DP = 3,200) were provided by Kuraray Co. Ltd., Tokyo, Japan. Acetic acid, $FeCl_3{\cdot}6H_2O$, $FeCl_2{\cdot}4H_2O$, and sodium hydroxide were purchased from Wako, Osaka, Japan. All the reagents were used as received without further purification.

Preparation of PVA nanofibers

PVA solutions were prepared by dissolving PVA in acetic acid aqueous solution at 90°C with constant stirring for at least 4 h. The electrospinning setup (Kato Tech, Kyoto, Japan) used in this study consists of a syringe with a flat-end metal needle (1.20-mm inner diameter, NN-1838 N, Terumo, Tokyo, Japan), a syringe pump for controlled the feeding rate, a grounded cylindrical stainless steel mandrel, and a high-voltage DC power supply. In a typical electrospinning process, PVA solution was transferred into a syringe and delivered to the tip of the syringe needle by the syringe pump at a constant feed rate (1.0 ml/h). A 12-kV positive voltage was applied to the PVA solution via the stainless steel syringe needle. The subsequently ejected polymer fiber was collected on the rotating cylindrical stainless steel mandrel, which was rotated during the electrospinning process (150 rpm). The distance between the tip of the needle and the surface of the mandrel was about 14 cm. The PVA nanofibers were vacuumed at room temperature for 24 h and thermal-treated at 180°C for 5 min.

Preparation of hollow α-Fe_2O_3 nanofibers

$FeCl_3{\cdot}6H_2O$ and $FeCl_2{\cdot}4H_2O$ were dissolved in 8 ml of distilled water, and the aqueous solution was degassed by N_2. The PVA nanofiber mat (0.5 mg) was immersed within the degassed aqueous solution of ferrous and ferric ions and stood for 1 h. After 1 h, NaOH aqueous solution (0.5 ml) was added slowly and the mixture was heated to 70°C for 60 min. After cooling to room temperature, the PVA-Fe_3O_4 composite mat was washed with water and dried *in vacuo* for 12 h.

As shown in Figure 1, the PVA-Fe_3O_4 composite mat was annealed in a tube furnace (GSL-1600X-80, Kejing, Hefei, China) at 600°C for 4 h under air to remove the PVA template and form hollow α-Fe_2O_3 nanofibers.

Characterization

Fiber morphology of the electrospun fibers was characterized using scanning electron microscopy (SEM) (SU1510, Hitachi Co. Ltd., Tokyo, Japan) and field-emission scanning electron microscopy (FE-SEM) (JSM-6700 F, JEOL, Akishima-shi, Japan) with an energy-dispersive X-ray spectrometer (EDS). Differential scanning calorimeter (DSC) (Q200, TA Instruments Inc., New Castle, USA) was used to characterize the thermal properties of the electrospun PVA mats. A piece of PVA mat (2 to 5 mg) was placed in an aluminum sample pan and heated from 30°C to 350°C at 10°C/min under N_2. Weight loss behavior was tested by thermogravimetric (TG) analysis (SDT Q600, TA Instruments Inc., New Castle, USA) (air, 10°C/min). The chemical structure of nanofibers was conducted with a Fourier transform infrared (FT-IR) reflection spectroscopy (NICOLET, Thermo Fisher Scientific, Waltham, USA), and a X-ray powder diffractometer (XRD) (D8 Advance, Bruker, Karlsruhe, Germany) operated in the reflection mode with Cu-Kα radiation in the 2θ range of 10° to 80° with a rate of 4°/min. Batch adsorption experiments were conducted and recorded by ultraviolet-visible spectra (U-3010, Hitachi Co. Ltd., Tokyo, Japan).

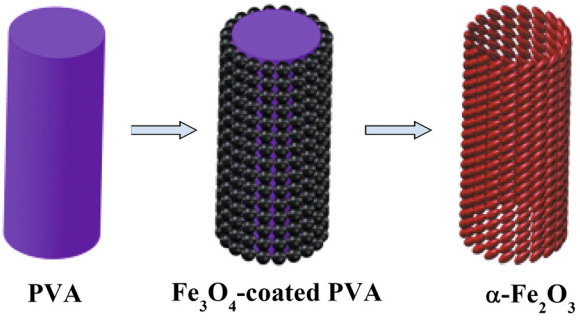

Figure 1 Schematic synthetic strategy for hollow α-Fe_2O_3 nanofibers.

Results and discussions

Deposition of Fe_3O_4 nanoparticles on PVA nanofibers

The formation of Fe_3O_4 on the PVA nanofibers can be monitored by the FT-IR spectra and XRD pattern. Figure 2 shows FT-IR spectra of as-spun PVA nanofibers, PVA nanofibers after heat treatment, and PVA nanofibers deposited with magnetite layer together with its XRD pattern. A broad characteristic peak at 3,300 cm^{-1} attributed to the -OH stretching vibration of PVA [13]. Compared to Figure 2a, no new absorbance band was observed in the spectrum of PVA nanofibers after heat treatment (Figure 2b), indicating only the physical changes that occur in the heat treatment process. In Figure 2c, the absorption peak at 567 cm^{-1} as the characteristic peak of Fe-O bonds in Fe_3O_4 was observed [24], indicating that successful hydrothermal synthesis of Fe_3O_4 on the surface of PVA nanofibers. Moreover, the formation of Fe_3O_4 was further confirmed by the characteristic peaks observed in the XRD pattern. As shown in Figure 2, the XRD pattern of PVA nanofibers deposited with magnetite layer showed five diffraction peaks at 2θ of 30.2°, 35.6°, 43.3°, 53.5°, and

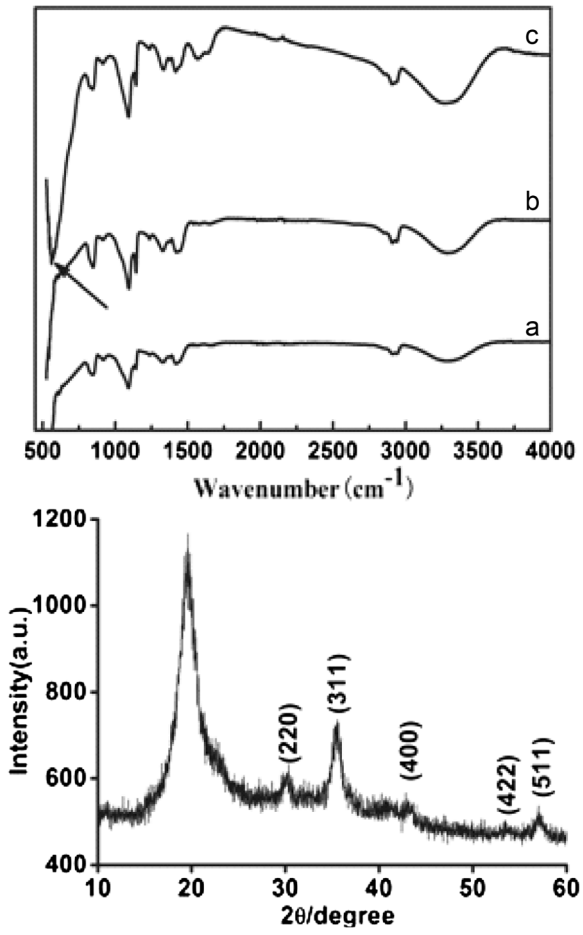

Figure 2 Infrared spectra of PVA nanofibers. **(a)** As-spun; **(b)** after thermal treatment; **(c)** coated with magnetite layer and its XRD pattern.

57.2°. These peak positions agree with (220), (311), (400), (422), and (511) crystallographic planes of the spinel phase of Fe_3O_4 [25].

Figure 3 shows the DSC curves of as-spun PVA nanofibers, PVA nanofibers after heat treatment, and PVA nanofibers coated with Fe_3O_4 nanoparticles. The enthalpy of 100% crystalline PVA is 138.6 J/g [26]. From Table 1, the crystallinity of as-spun PVA nanofibers is 51.4%. After heat treatment at 180°C for 5 min, the crystallinity of PVA nanofibers increased to 56.7%, which is due to the removal of H_2O in the PVA matrix, so that the hydrogen bonding between PVA macromolecules is enhanced, thereby promote the crystallization. After the hydrothermal reaction for the deposition of Fe_3O_4 nanoparticles, the crystallinity of PVA-Fe_3O_4 composite decreased from 56.7% to 31.4%. Meanwhile, the melting point slightly decreased from 223°C to 222°C. During the process of hydrothermal synthesis, some water molecules squeezed into the PVA molecular chains, weakened the hydrogen bonding of -OH groups.

Table 1 The melting point and enthalpy of PVA nanofibers

PVA nanofibers	Tm (°C)	ΔH (J/g)
As-spun fibers	227	71.3
After thermal treatment	223	78.5
PVA-Fe_3O_4 composite fibers	222	43.5

Hollow α-Fe_2O_3 nanofibers

Figure 4 shows the TG curves of PVA nanofibers before and after the hydrothermal reaction. After the heat treatment, PVA nanofibers reveal good thermal stability below 229°C. Weight loss occurs in the region of 240°C to 350°C, probably because of dehydration of hydroxyl groups within the skeleton PVA molecules. Weight loss between 350°C to 470°C was mainly induced by the decomposition of C-C skeleton. Over 470°C, the weight of PVA basically unchanged which implies that PVA has

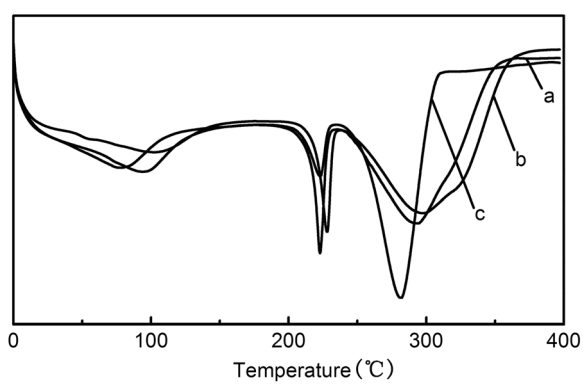

Figure 3 DSC curves of PVA nanofibers **(a)** as-spun, **(b)** after thermal treatment, and **(c)** coated with Fe_3O_4 magnetic nanoparticles.

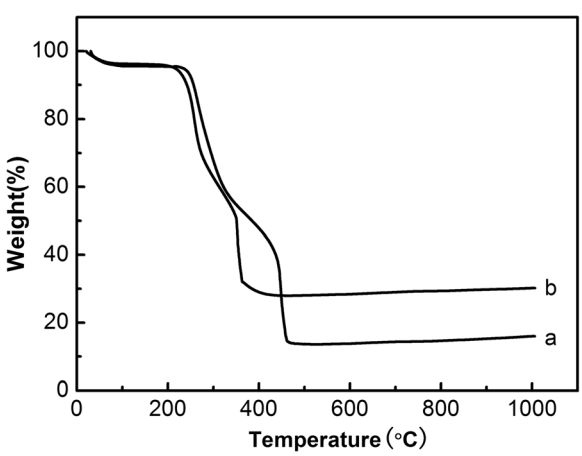

Figure 4 Thermogravimetric analysis curves of PVA nanofibers **(a)** after heat treatment and **(b)** coated with Fe_3O_4 magnetic nanoparticles.

been completely removed via calcination. In Figure 3b, PVA-Fe_3O_4 composite fibers showed a difference of 17 wt% in resultant weight over 500°C compared to PVA nanofibers which generated nonwoven fabrics of iron oxide.

Figure 5a shows the XRD pattern of the calcined product prepared at 600°C for 4 h under air. The diffraction peaks at 2θ of 24.1°, 33.2°, 35.6°, 40.8°, 49.4°, 54.1°, 57.6°, 62.4°, and 64.0° correspond to (012), (104), (110), (006), (024), (116), (018), (214), and (300) crystallographic planes of hematite structure of α-Fe_2O_3 by comparison with JCPDS card files number 87-1166 (a = 5.038 Å, c = 13.756 Å) [27]. The strong and sharp diffraction peaks indicate good crystallinity of the calcined product. No characteristic peaks from impurities are detected. The formation of Fe_2O_3 was further confirmed by EDS pattern (Figure 5b) of the calcined product. Fe and O peaks can be clearly seen.

As shown in Figure 6a, the as-spun PVA nanofibers with an average diameter of 311 ± 66 nm are straight and reveal uniform and smooth surfaces. After heat treatment, PVA nanofibers are bent and the diameter of the fiber becomes slightly thicker, increased to 328 ± 55 nm, which may be due to the annealing during the heat treatment process. During the deposition process of magnetite, the color of nanofiber mat was changed from white to pale brown. The SEM image revealed a uniform deposition of Fe_3O_4 layer onto the surface of PVA nanofibers and no formation of large magnetite particles (Figure 6c). The average diameter of Fe_3O_4 nanoparticle-coated PVA nanofibers was 380 ± 53 nm; thus, the layer thickness of Fe_3O_4 nanoparticles deposited on PVA nanofibers was about 26 nm. The uniform deposition of Fe_3O_4 layer is mainly attributed to the complexation of iron ions or Fe_3O_4 nanoparticles with the hydroxyl groups in PVA. After calcination at 600°C for 4 h under air, intact nanofibrous morphology remained, but hollow structure was approached (as indicated by an arrow in Figure 6d). With the calcination temperature increased gradually, PVA nanofibers decomposed, interconnected Fe_3O_4 nanoparticles maintained the fibrous morphology, and eventually transformed to α-Fe_2O_3 nanofibers with hollow structure.

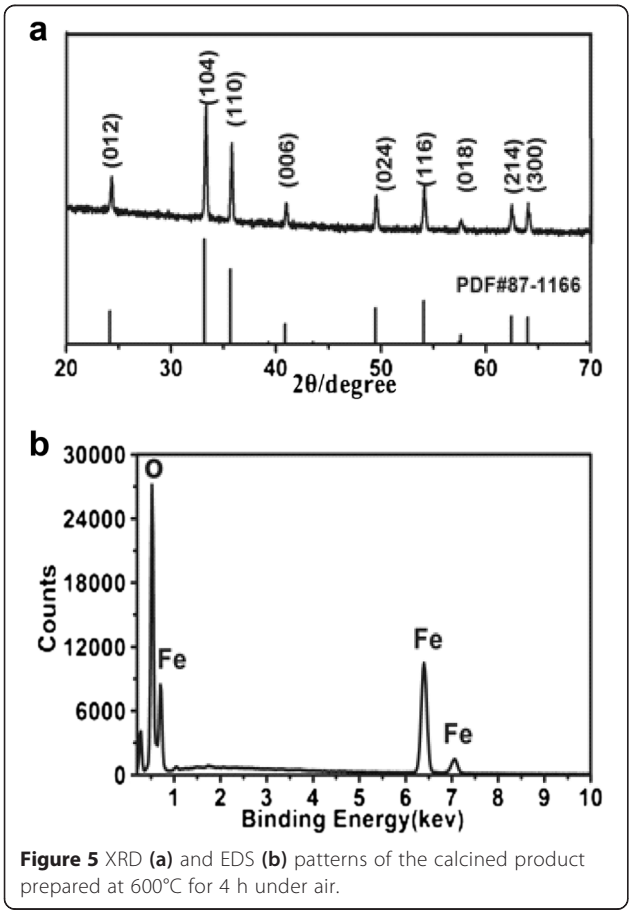

Figure 5 XRD **(a)** and EDS **(b)** patterns of the calcined product prepared at 600°C for 4 h under air.

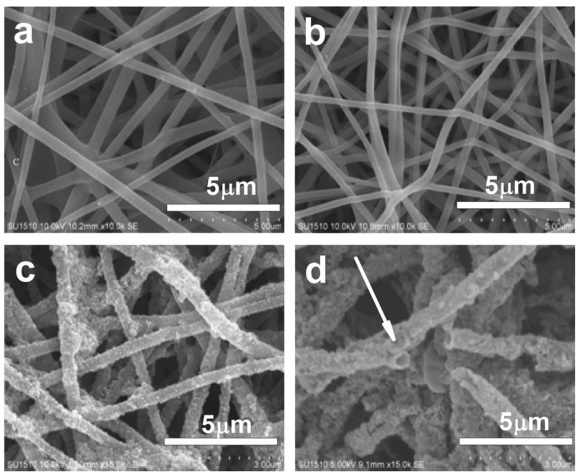

Figure 6 SEM images of PVA nanofibers. **(a)** As-spun; **(b)** after thermal treatment; **(c)** coated with Fe_3O_4 magnetic nanoparticles; **(d)** after calcination at 600°C for 4 h under air.

The geometrical parameters of PVA nanofibers, such as the average diameter of nanofibers, the porosity, and the thickness of fiber assembles, would significantly influence the resultant morphology of α-Fe_2O_3 nanofibers. Furthermore, the hydrothermal reaction conditions, such as temperature and ion concentration, should have similar effects. Here, the effect of ion concentration on the resultant morphology of α-Fe_2O_3 was investigated. Other parameters will be reported in the following full paper.

α-Fe_2O_3 with diverse shapes was prepared from the same calcination process due to the different ion concentrations in hydrothermal reaction as shown in Table 2. In Figure 7, when the ion concentration is low, continuous fibers of interconnected nanorods were approached

Table 2 Ion concentration in the hydrothermal synthesis

α-Fe_2O_3	$FeCl_3 \cdot 6H_2O$ (μmol)	$FeCl_2 \cdot 4H_2O$ (μmol)	NaOH (mol)
a	2.11	1.05	2.12
b	21.1	10.5	21.2
d	211	105	212

(Figure 7a), similar to the reported work [11]. When Fe^{3+} ion content increases to 21.1 μmol, novel hollow α-Fe_2O_3 nanofibers made of rice-like nanorods were prepared as shown in a representative high-resolution FE-SEM image (Figure 7b). In Figure 7c, hollow structure of α-Fe_2O_3 nanofibers can be clearly seen and abundant rice-like nanorods with the mean size of 60 ± 17 nm can be found. The hollow α-Fe_2O_3 nanofibers with hierarchical structure will find wide applications in photocatalyst, heavy metal ion detection, and lithium-ion battery due to the specific structure. However, tenfold increase in ion concentration resulted in only aggregates of α-Fe_2O_3 nanoparticles without fibrous morphology.

Magnetic response and absorption for dyes

Nanostructured α-Fe_2O_3 displays weak ferromagnetic behavior at room temperature [28]. The M-H curves revealed in Figure 8 show a nonlinear and reversible behavior with a weak magnetic hysteresis loop. This was related to the fine crystallite sizes of α-Fe_2O_3 nanorods. The as-prepared hollow α-Fe_2O_3 nanofibers made of rice-like nanorods (Figure 7b) exhibited a robust saturation magnetization of 24.4 $emu \cdot g^{-1}$, higher than 10.2 $emu \cdot g^{-1}$ of solid fibers (Figure 7a) and that in the reported work [29], which should be ascribed to the hollow fiber structure and well-defined rice-like shape of α-Fe_2O_3.

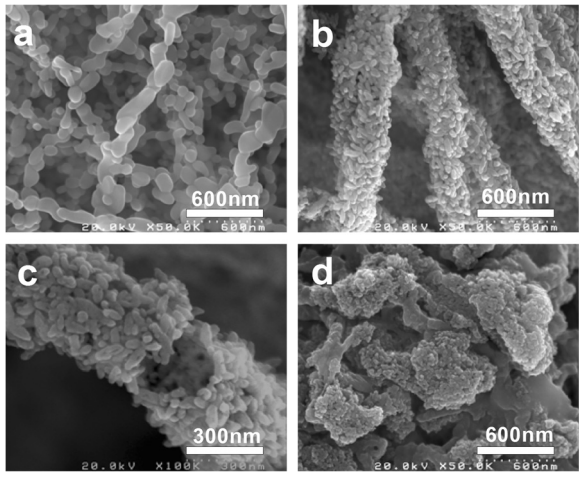

Figure 7 FE-SEM images of α-Fe_2O_3 with diverse shapes prepared at different ion concentrations. **(a)** a in Table 2; **(b, c)** b in Table 2; **(d)** d in Table 2.

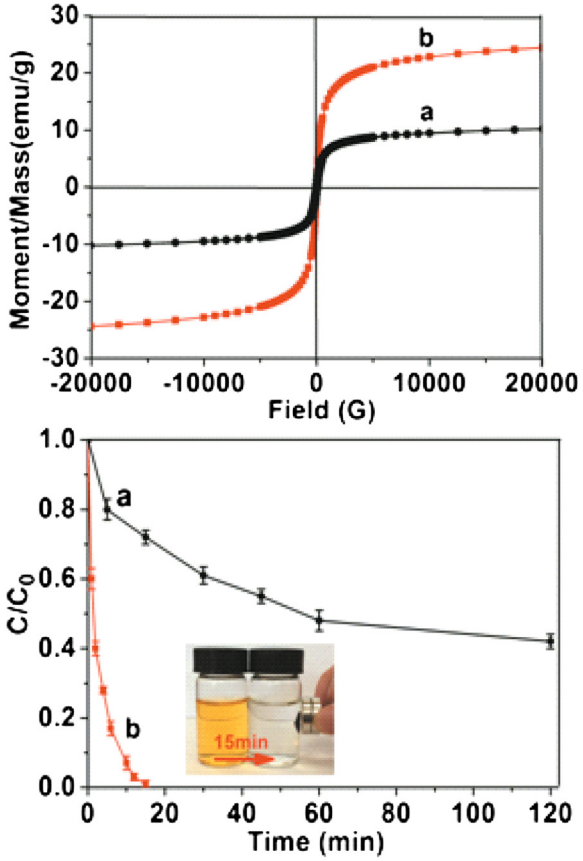

Figure 8 M-H curves and the adsorption capacity of MO of hollow α-Fe_2O_3 nanofibers. Magnetic hysteresis loops of α-Fe_2O_3 fibers measured at 300 K and the C/C_0 versus time plots for adsorption of MO solution using **(a)** solid fibers and **(b)** hollow fibers made of rice-like nanorods; the inset shows the magnetic response of hollow α-Fe_2O_3 fibers made of rice-like nanorods after adsorption of MO for 15 min.

As expected, hollow α-Fe_2O_3 nanofibers made of rice-like nanorods which combined the porous structure and the magnetic performance demonstrated efficient adsorption for organics and fast magnetic separation property. Methyl orange (MO; 2×10^{-5} M) was employed for typical organic pollutants in adsorption test. Figure 8 indicates that the adsorption capacity of MO of hollow α-Fe_2O_3 nanofibers was 93% for 10 min and could achieve almost complete adsorption of MO in 15 min (insert image of Figure 8) while solid α-Fe_2O_3 fibers revealed much slower adsorption rate. Moreover, hollow α-Fe_2O_3 nanofibers after adsorption could be separated facilely using an external magnet without any tedious separation process, which is of great importance for real applications.

Recently, environmental cleanup has been one of the most active areas in photocatalysis. An ideal photocatalyst should be stable, inexpensive, nontoxic, and, of course, highly photoactive [30]. Fe_2O_3 stands out with

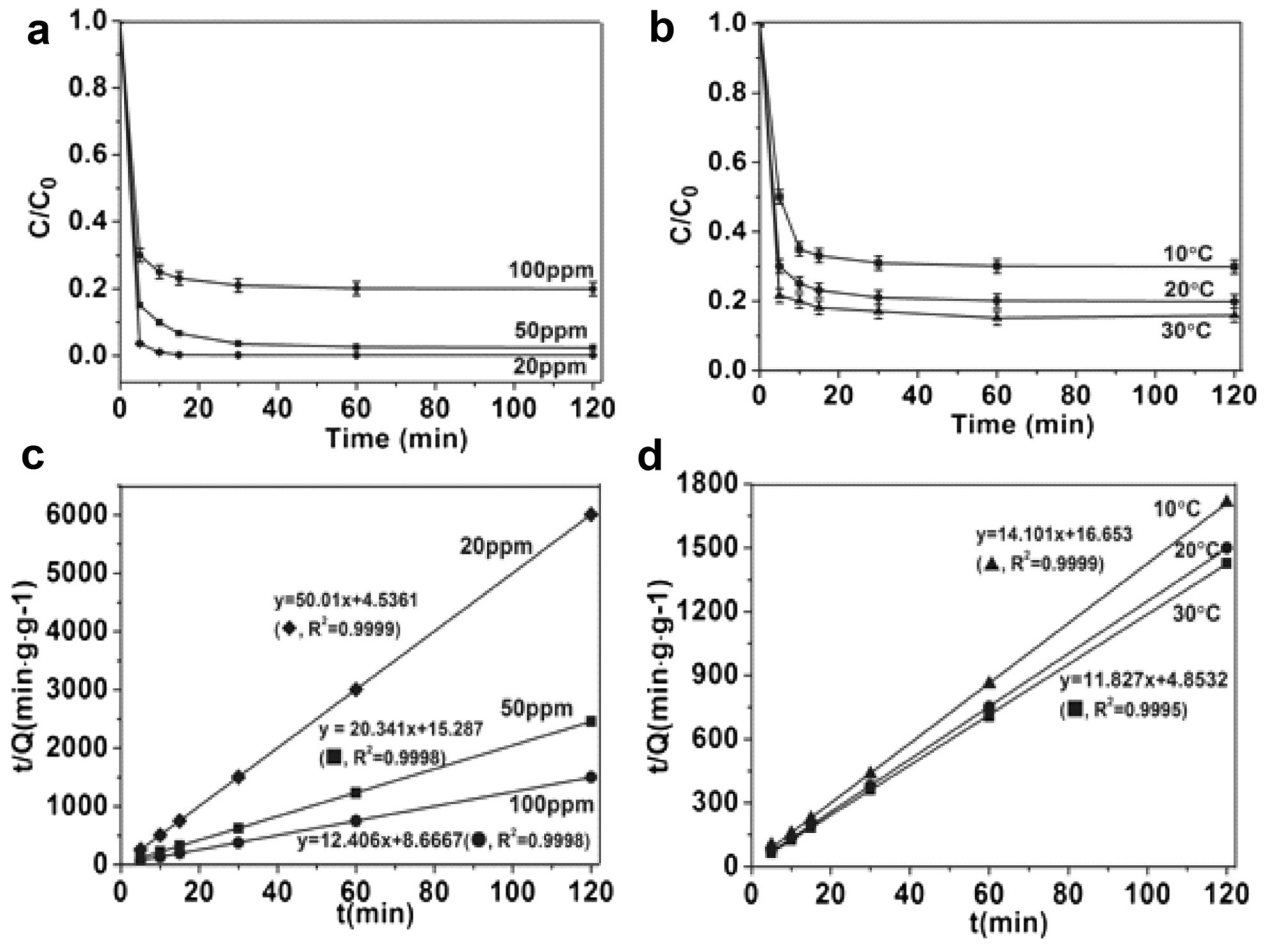

Figure 9 Adsorption curves and kinetics of hollow α-Fe_2O_3 fibers made of rice-like nanorods to MO. Different initial MO concentrations **(a, c)** and temperatures **(b, d)**.

its nearly ideal bandgap of 2.2 eV and its high photochemical stability in aqueous solutions [31]. Yu et al. reported that degradation pathways of MO by using well-defined α-Fe_2O_3 nanocrystals involve both *N*-demethylation and the cleavage of conjugated chromophores [23]. To clear the adsorption kinetics of MO by using hollow α-Fe_2O_3 nanofibers made of rice-like nanorods, the effects of initial MO concentration and temperature were investigated systematically. As shown in Figure 9, at lower initial MO concentration (Figure 9a) or higher temperature (Figure 9b), better MO degradation performance was observed. Lagergren pseudo-second-order kinetic model was adopted to describe the adsorption process. k_2 is the adsorption rate constant, Q_e is the equilibrium absorption capacity:

$$\frac{t}{Q} = \frac{1}{k_2 Q_e^2} + \frac{t}{Q_e}$$

Figure 9c shows that the adsorption curves to MO of hollow α-Fe_2O_3 nanofibers at different initial MO concentrations, which are based on the Lagergren pseudo-second-order kinetic equation. The change in initial MO concentration results in different molar ratio of hollow α-Fe_2O_3 nanofibers to MO, finally lead to varying k_2. When initial MO concentration increased from 20 to 50 ppm, k_2

Table 3 Adsorption rate constant k_2 at different initial MO concentration and temperature

Adsorption condition	Initial MO concentration/ppm (at 20°C)			Temperature/°C (at 100 ppm)		
	20	50	100	10	20	30
k_2	551.35	27.07	17.76	11.94	17.76	28.82

dramatically reduced from 551.35 to 27.07 min^{-1}. When the initial MO concentration is 100 ppm, k_2 is 17.759 min^{-1}, the equilibrium absorption capacity Q_e is 80.6 $mg{\cdot}g^{-1}$. The increase of the initial MO concentration is negative to the adsorption rate, and this coincides with Figure 9a. The temperature of batch adsorption also affects the adsorption kinetics. As revealed in Figure 9d and Table 3, a 2.4-fold increase in k_2 was achieved with the increase of experimental temperature from 10°C to 30°C.

Conclusions

Novel hollow α-Fe_2O_3 nanofibers made of rice-like nanorods were successfully synthesized via a simple hydrothermal reaction on PVA nanofiber template followed by calcination. The crystallographic structure and the morphology of the as-prepared α-Fe_2O_3 nanofibers were conformed by XRD, EDS, and FE-SEM. Moreover, hollow α-Fe_2O_3 fiber assembles exhibited magnetic responsive performance, as well as efficient adsorption for methyl orange in water which follows Lagergren pseudo-second-order kinetics. This work provided a versatile strategy for further design and development of functional nanofiber-nanoparticle composites towards various applications.

Competing interests

The authors declare that they have no competing interests.

Authors' contributions

QG and MQG designed the experiments. JL and XYW carried out the electrospinning, calcination, and dye adsorption experiments. CXG and QG contributed to data analysis. All authors read and approved the final manuscript.

Acknowledgements

We acknowledge financial support from the National High-tech R&D Program of China (863 Program, Grant Number: 2012AA030313), State Key Laboratory of Molecular Engineering of Polymers(Fudan University) (K2015-23), and Fundamental Research Funds for the Central Universities of China (No. JUSRP11444).

Author details

[1]Key Laboratory of Science and Technology of Eco-Textiles, Ministry of Education, Jiangnan University, 1800 Lihu Road, Wuxi 214122, China. [2]State Key Laboratory of Molecular Engineering of Polymers, Department of Macromolecular Science and Laboratory of Advanced Materials, Fudan University, 220 Handan Road, Shanghai 200438, China. [3]Institute of Orthopaedics, The First Affiliated Hospital, Soochow University, 708 Renmin Road, Suzhou 215006, China.

Received: 6 November 2014 Accepted: 21 March 2015
Published online: 14 April 2015

References

1. Fan HM, Yi JB, Yang Y, Kho KW, Tan HR, Shen ZX, et al. Single-crystalline MFe_2O_4 nanotubes/nanorings synthesized by thermal transformation process for biological applications. ACS Nano. 2009;3(9):2798–808.
2. Son SJ, Reichel J, He B, Schuchman M, Lee SB. Magnetic nanotubes for magnetic-field-assisted bioseparation, biointeraction, and drug delivery. J Am Chem Soc. 2005;127(20):7316–7.
3. Zheng Y, Cheng Y, Wang Y, Bao F, Zhou L, Wei X, et al. Quasicubic α-Fe_2O_3 nanoparticles with excellent catalytic performance. J Phys Chem B. 2006;110(7):3093–7.
4. Barroso M, Cowan AJ, Pendlebury SR, Grätzel M, Klug DR, Durrant JR. The role of cobalt phosphate in enhancing the photocatalytic activity of α-Fe_2O_3 toward water oxidation. J Am Chem Soc. 2011;133(38):14868–71.
5. Ouyang J, Pei J, Kuang Q, Xie Z, Zheng L. Supersaturation-controlled shape evolution of α-Fe_2O_3 nanocrystals and their facet-dependent catalytic and sensing properties. ACS Appl Mater Interfaces. 2014;6(15):12505–14.
6. Chen J, Xu LN, Li WY, Gou XL. α-Fe_2O_3 nanotubes in gas sensor and lithium-ion battery applications. Adv Mater. 2005;17(5):582–6.
7. Zhu X, Zhu Y, Murali S, Stoller MD, Ruoff RS. Nanostructured reduced graphene oxide/Fe_2O_3 composite as a high-performance anode material for lithium ion batteries. ACS Nano. 2011;5(4):3333–8.
8. Sun Z, Yuan H, Liu Z, Han B, Zhang X. A highly efficient chemical sensor material for H_2S: α-Fe_2O_3 nanotubes fabricated using carbon nanotube templates. Adv Mater. 2005;17(24):2993–7.
9. Long NV, Yang Y, Yuasa M, Thi CM, Cao Y, Nann T, et al. Gas-sensing properties of p-type α-Fe_2O_3 polyhedral particles synthesized via a modified polyol method. RSC Adv. 2014;4(16):8250–5.
10. Liu R, Wang Q, Shen X, Yang X, Wu D, Cui X. Preparation of α-Fe_2O_3 nanotubes by calcination of electrospun precursors. J Nanosci Nanotechnol. 2014;14(3):2670–3.
11. Zhu Y, Zhang JC, Zhai J, Jiang L. Preparation of superhydrophilic α-Fe_2O_3 nanofibers with tunable magnetic properties. Thin Solid Films. 2006;510(1):271–4.
12. Ren T, He P, Niu W, Wu Y, Ai L, Gou X. Synthesis of α-Fe_2O_3 nanofibers for applications in removal and recovery of Cr (VI) from wastewater. Environ Sci Pollut Res. 2013;20(1):155–62.
13. Gao Q, Takizawa J, Kimura M. Hydrophilic non-wovens made of cross-linked fully-hydrolyzed poly (vinyl alcohol) electrospun nanofibers. Polymer. 2013;54(1):120–6.
14. Gao Q, Meguro H, Okamoto S, Kimura M. Flexible tactile sensor using reversible deformation of poly(3-hexylthiophene) nanofiber assemblies. Langmuir. 2012;28(51):17593–6.
15. Gao C, Rahaman MN, Gao Q, Teramoto A, Abe K. Robotic deposition and in *vitro* characterization of 3D gelatin-bioactive glass hybrid scaffolds for biomedical applications. J Biomed Mater Res A. 2013;101(7):2027–37.
16. Zhou J, Gao Q, Fukawa T, Shirai H, Kimura M. Macroporous conductive polymer films fabricated by electrospun nanofiber templates and their electromechanical properties. Nanotechnology. 2011;22(27):275501.
17. Ji X, Wang P, Su Z, Ma G, Zhang S. Enabling multi-enzyme biocatalysis using coaxial-electrospun hollow nanofibers: redesign of artificial cells. J Mater Chem B. 2014;2(2):181–90.
18. Cao J, Zhang T, Li F, Yang H, Liu S. Enhanced ethanol sensing of SnO_2 hollow micro/nanofibers fabricated by coaxial electrospinning. New J Chem. 2013;37(7):2031–6.
19. Angeles M, Cheng HL, Velankar SS. Emulsion electrospinning: composite fibers from drop breakup during electrospinning. Polym Adv Technol. 2008;19(7):728–33.
20. Xu X, Zhuang X, Chen X, Wang X, Yang L, Jing X. Preparation of core-sheath composite nanofibers by emulsion electrospinning. Macromol Rapid Commun. 2006;27(19):1637–42.
21. Cao CY, Qu J, Yan WS, Zhu JF, Wu ZY, Song WG. Low-cost synthesis of flowerlike α-Fe_2O_3 nanostructures for heavy metal ion removal: adsorption property and mechanism[J]. Langmuir. 2012;28(9):4573–9.
22. Kay A, Cesar I, Grätzel M. New benchmark for water photooxidation by nanostructured α-Fe_2O_3 films. J Am Chem Soc. 2006;128(49):15714–21.
23. Zhou X, Xu Q, Lei W, Zhang T, Qi X, Liu G, et al. Origin of tunable photocatalytic selectivity of well-defined α-Fe_2O_3 nanocrystals[J]. Small. 2014;10(4):674–9.
24. Pan C, Hu B, Li W, Sun YI, Ye H, Zeng X. Novel and efficient method for immobilization and stabilization of β-d-galactosidase by covalent attachment onto magnetic Fe_3O_4-chitosan nanoparticles. J Mol Catal B: Enzym. 2009;61(3):208–15.
25. Pimpha N, Chaleawlert-umpon S, Sunintaboon P. Core/shell polymethyl methacrylate/polyethyleneimine particles incorporating large amounts of iron oxide nanoparticles prepared by emulsifier-free emulsion polymerization. Polymer. 2012;53(10):2015–22.
26. Wang N, Ji S, Li J, Zhang R, Zhang G. Poly (vinyl alcohol)-graphene oxide nanohybrid "pore-filling" membrane for pervaporation of toluene/n-heptane mixtures. J Membr Sci. 2014;455:113–20.
27. Yang XY, Li Y, Van Tendeloo G, Xiao FS, Su BL. One-pot synthesis of catalytically stable and active nanoreactors: encapsulation of size-controlled nanoparticles within a hierarchically macroporous core@ ordered mesoporous shell system[J]. Adv Mater. 2009;21(13):1368–72.

28. Mitra S, Das S, Mandal K, Chaudhuri S. Synthesis of a α-Fe_2O_3 nanocrystal in its different morphological attributes: growth mechanism, optical and magnetic properties. Nanotechnology. 2007;18(27):275608.
29. Wang X, Zhang L, Ni Y, Hong J, Cao X. Fast preparation, characterization, and property study of α-Fe_2O_3 nanoparticles via a simple solution-combusting method. J Phys Chem C. 2009;113(17):7003–8.
30. Beydoun D, Amal R, Low G, McEvoy S. Role of nanoparticles in photocatalysis. J Nanopart Res. 1999;1(4):439–58.
31. Chirita M, Banica R, Ieta A, Grozescu I. Fe-EDTA thermal decomposition, a route to highly crystalline hematite (alpha Fe_2O_3) nanoparticle synthesis[J]. Part Sci Technol. 2010;28(3):217–25.